Experimental Evaluation of Super-Gaussian-Shaped Random FM Waveforms

Matthew B. Heintzelman, Thomas J. Kramer, Shannon D. Blunt
Radar Systems Lab (RSL), University of Kansas, Lawrence KS

***Abstract* – The class of noise radar waveform known as random frequency modulation (RFM) has been used to enable a variety of new sensing capabilities. It was also recently shown in simulation that a more compact design spectral template translates to better spectral containment, with a trade-off of emerging close-in "persistent" sidelobes. Here we take the next step of implementing in hardware sets of RFM waveforms designed in this manner to assess their loopback behavior and subsequently characterize their performance with open-air experimental measurements.**

Keywords – waveform design, spectral containment, noise radar

I. INTRODUCTION

While RFM waveforms (also known as FM noise) can be traced back to the 1956 patent application of Whiteley and Adrian [1] and other work since [2-5], our particular focus is on RFM waveforms that employ spectrum shaping, which provides multiple practical benefits [6]. These include *a*) managing range sidelobes due to the Fourier relationship between waveform autocorrelation and spectral density [7], *b*) controlling out-of-band roll-off to reduce transmitter distortion effects [8], and *c*) possibly incorporating transmit notching to reduce radar interference to other spectrum users [9].

Of course, these attributes/capabilities of waveform spectrum shaping can sometimes be in conflict with one another, as is the case here. Specifically, it is well known that the Fourier transform of a Gaussian shape yields another Gaussian. Therefore, if the spectral density is made to conform to a Gaussian template, then the associated autocorrelation would as well, and consequently possess no sidelobes (theoretically at least). While Gaussian spectral roll-off is far more compact than the sinc "spectral skirt" realized by polyphase codes [10], it is still considerably broader than the extreme spectral compactness of a linear FM (LFM) chirp, which remains the standard for wideband applications.

It is worth noting that traditional noise radar (e.g. [11-13]) can readily achieve wideband operation, though the key difference with wideband LFM operation is that the latter can be generated at high-power for long-range applications due to its FM structure, while traditional noise radar possesses significant amplitude modulation (AM). To facilitate the use of noise radar's high dimensionality for high-power wideband operation it therefore becomes necessary to determine how RFM can be employed with even greater spectral compactness, since a factor of 2× to 4× expansion beyond 3-dB bandwidth to account for Gaussian spectral roll-off becomes infeasible as bandwidth gets large.

It was recently shown [14] that the Gaussian template can be subsumed into the super-Gaussian framework from optics. In so doing, control of spectral containment can be achieved with a single selectable parameter. In [14] the super-Gaussian template was incorporated into the temporal template error (TTE) RFM design framework from [15], with simulated results provided to assess the performance trade-space. Here we instead use the pseudo-random optimized (PRO) FM [16] approach to illustrate the utility across different RFM methods while also evaluating practical behavior via experimental loopback and open-air measurements.

II. PRO-FM OPTIMIZATION REVIEW

The PRO-FM method for spectrally-shaped RFM waveform design relies on an alternating projections optimization process [16]. Given a selected power spectral density (PSD) design template $|G(f)|^2$ and an independent random initialization for the mth waveform (within a set of M) denoted as $p_{0,m}(t)$, the sequential process

$$r_{k+1,m}(t) = \boldsymbol{\mathcal{F}}^{-1}\{|G(f)| \exp\left(j\angle\left\{\boldsymbol{\mathcal{F}}\{p_{k+1,m}(t)\}\right\}\right)\} \qquad (1)$$

and

$$p_{k+1,m}(t) = u(t) \exp\left(j\angle\{r_{k+1,m}(t)\}\right) \qquad (2)$$

is repeated for some number of iterations K. Here $u(t)$ is the rectangular pulse envelope with time support on $[0, T]$, the operations $\boldsymbol{\mathcal{F}}\{\cdot\}$ and $\boldsymbol{\mathcal{F}}^{-1}\{\cdot\}$ are the Fourier and inverse Fourier transforms, respectively, and $\angle\{\cdot\}$ extracts the phase of the argument.

Since the implementation of (1) and (2) requires discretization of the signals involved, and finite time support implies theoretically infinite spectral support, an adequate degree of "over-sampling" is necessary. It is convenient to define the degree of over-sampling relative to 3-dB bandwidth, though any such measure could be selected. In discretized form, (1) can be computed efficiently using FFTs and IFFTs.

III. SUPER-GAUSSIAN DESIGN TEMPLATE

In PRO-FM and related spectrum-shaping RFM approaches [15-17] the PSD design template $|G(f)|^2$ was chosen to be Gaussian-shaped to provide a corresponding Gaussian-shaped autocorrelation that has no sidelobes (or at least the closest approximation thereof that is achievable by a rectangular pulsed FM structure). In reality, for pulse width T and 3-dB bandwidth B, the associated time-bandwidth product TB realizes sidelobes roughly approaching $20\log_{10}(TB)$ on a per-pulse basis (from a root mean-square (RMS) perspective), with an additional $10\log_{10}(M)$ sidelobe suppression achieved due to incoherent averaging when performing slow-time processing across a set of unique RFM waveforms.

This work was supported in part by the Office of Naval Research under Contract #N00014-20-C-1006 and Sandia National Laboratories under Contract #2237007.
DISTRIBUTION STATEMENT A. Approved for Public Release. DCN # 43-8714-21.

While the Gaussian template provides fairly low RFM sidelobes, it does so by requiring a roughly 2× to 4× inclusion of spectral content beyond the 3-dB bandwidth due to modest roll-off (to avoid degradation from aliasing). For bandwidths measured in 10s of MHz this factor may be feasible, but for bandwidths on the order of 100s of MHz up to GHz such an expansion to account for spectral roll-off becomes prohibitive.

To that end, the super-Gaussian template was recently considered in this RFM waveform design context [14]. The super-Gaussian function, which originated in the field of optics, is described in [18] and takes the general form

$$f(x) = A \exp\left(-\frac{1}{2} \left| \frac{x-\gamma}{\sigma} \right|^n \right), \tag{3}$$

where σ and n are real and positive, A is an arbitrary scaling used to set the desired power level, and the function is centered at γ. For the case where $n = 2$, the function in (3) simplifies to the standard Gaussian template. It can also be analytically shown that, in the limit as n approaches infinity, the shape of (3) approaches a rectangular function. While being well-contained spectrally, a rectangular template would obviously induce a sinc roll-off in the autocorrelation, just like LFM.

By adjusting the exponent n, the trade-space between achieving lower autocorrelation sidelobes and better spectral containment can be explored, as demonstrated in Figs. 1 and 2 for selected values of n (the autocorrelations in Fig. 2 are computed via inverse Fourier transform of the spectral templates in Fig. 1). Each case has been peak-normalized to provide easy comparison.

In [14] the value of σ in (3) was individually set for each value of n so that the spectral templates for different cases all cross at the same peak-normalized power level, which corresponded to a normalized digital frequency of ±0.4 (within the ±0.5 limits). Doing so permitted comparison of how much "usable bandwidth" could be obtained for a fixed sample rate in the discretized design process.

In contrast, here (Fig. 1) we maintain the same 3-dB bandwidth, adjusting σ as necessary. This perspective alternatively necessitates different over-sampling to capture the same spectral roll-off level. Determining the appropriate value of σ is accomplished by rearranging (3) to obtain

$$\sigma = \frac{|x_0 - \gamma|}{(2\ln(2A))^{1/n}} = \frac{(B/2)}{(2\ln(2))^{1/n}}, \tag{4}$$

where x_0 is half the 3-dB bandwidth B, and we have simply set $\gamma = 0$ and $A = 1$.

The corresponding autocorrelation responses in Fig. 2 provide essentially the same range resolution, but still exhibit the emergence of persistent sidelobes close to the mainlobe that are not suppressed through slow-time incoherent averaging (as occurs for RFM having Gaussian-shaped spectrum [6]).

Fig. 3 then illustrates a simulated comparison in this context via the RMS average of autocorrelations from 5000 unique PRO-FM waveforms for each value of n (= 2, 8, 32). A constant $TB = 472$ is maintained, with a factor of 10 over-sampling used for optimization (overkill for higher n values, but provides consistent comparison). We observe that the Gaussian (n = 2) template has no persistent sidelobes and yields the lowest sidelobe floor, which unlike Fig. 2 occurs because this result is based on actual waveform responses (i.e. perfect template matching is not possible).

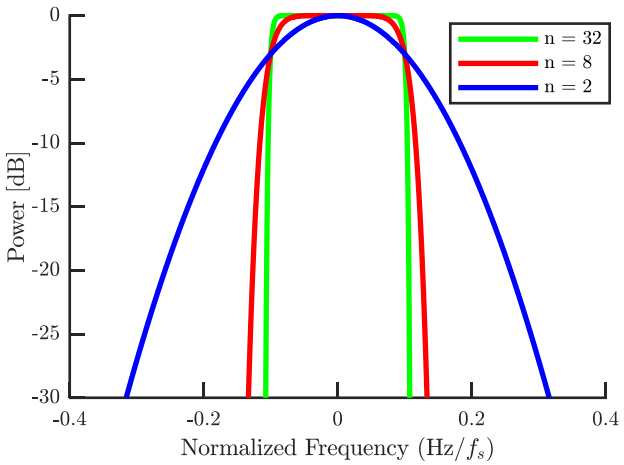

Fig. 1. Comparison of super-Gaussian spectral templates

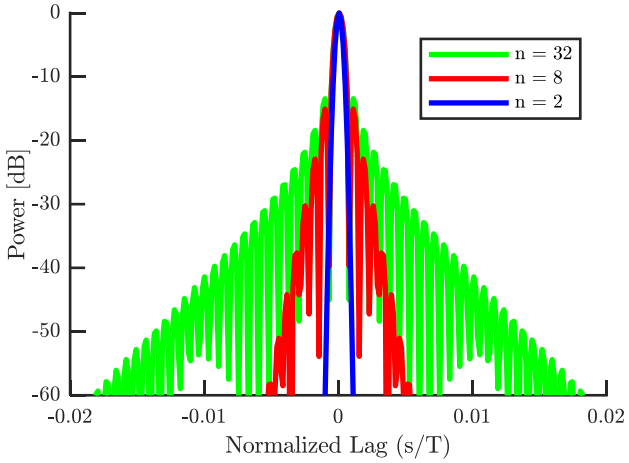

Fig. 2. Autocorrelation comparisons of templates in Fig. 1

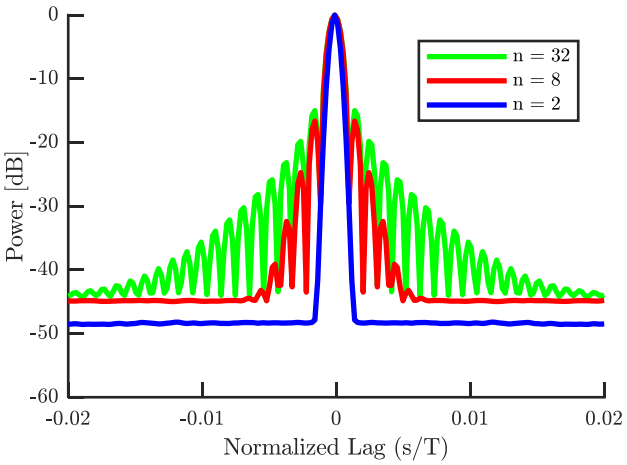

Fig. 3. RMS autocorrelation for 5000 unique PRO-FM waveforms generated using different super-Gaussian values of *n*

As expected from the template autocorrelations in Fig. 2, the n = 8 and 32 cases in Fig. 3 do realize persistent sidelobes. Like

the $n = 2$ case they also reach a sidelobe floor due to the use of actual waveforms. We observe this floor is about 3 dB higher than that of $n = 2$, an effect discussed in [14]. This floor region is where the incoherent sidelobes begin and therefore further suppression is achieved when slow-time processing is performed. Of course, the particular normalized delays where the floor starts gradually moves outward as more unique waveforms are slow-time processed due to the uncovering of additional close-in persistent sidelobes. Consequently, there is a clear trade-off between spectral containment, overall waveform dimensionality (over the entire CPI), and the level of sidelobe suppression that can be achieved.

IV. EXPERIMENTAL ANALYSIS

The set of 5000 unique PRO-FM waveforms used above were likewise employed for experimental assessment in hardware. The particular value of $TB = 472$ arises from using a pulse width of 6.67 μs and 3-dB bandwidth of 70.7 MHz at a center frequency of 3.55 GHz. This arrangement is clearly not in the wideband regime but is used here to begin examining the trade-space given available test equipment.

For each value of $n = 2$, 8 and 32, the corresponding set of 5000 unique waveforms was generated and captured in a loopback configuration using a pulse repetition frequency (PRF) of 50 kHz so that some degree of hardware-induced distortion characterization could be performed. From these measurements the autocorrelations, cross-correlations, and spectral densities are then evaluated, from the perspectives of both per-waveform (RMS) behavior and after coherent combination (slow-time processing).

Figs. 4, 5 and 6 show loopback autocorrelation results for the $n = 2$, 8, and 32 parameterizations, respectively. We see that the RMS peak sidelobe level (PSL) is –32.6 dB for the $n = 2$ case, –17.1 dB for the $n = 8$ case, and –15.4 dB for the $n = 32$ case. Of course, these values are a result of persistent sidelobes in the $n = 8$ and 32 cases (evident from the apparent lower mainlobe broadening in Figs. 5 and 6) and "shoulder lobes" on the mainlobe for $n = 2$ caused by hardware effects. If we exclude these very close-in components, the PSL values become –39.8 dB, –36.5 dB, and –36.2 dB for $n = 2$, 8 and 32, respectively. In short, outside of persistent sidelobes there is a modest trade-off in the incoherent sidelobe floor as n increases.

Table 1: PSL of RMS autocorrelations

	PSL (including persistent/shoulder sidelobes)	PSL (excluding persistent/shoulder sidelobes)
$n = 2$	–32.6 dB	–39.8 dB
$n = 8$	–17.1 dB	–36.5 dB
$n = 32$	–15.4 dB	–36.2 dB

The coherent combination responses in Figs. 4-6 also bear consideration. These arise from slow-time coherent combining across each set of 5000 unique waveforms after pulse compression. All three cases realize $10 \log_{10}(5000) = 37$ dB of sidelobe suppression relative to the single waveform response.

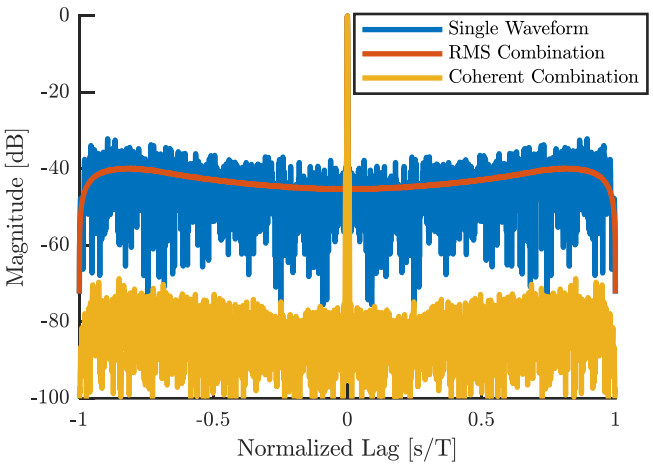

Fig. 4. Loopback autocorrelation results for 5000 unique PRO-FM waveforms generated using $n = 2$

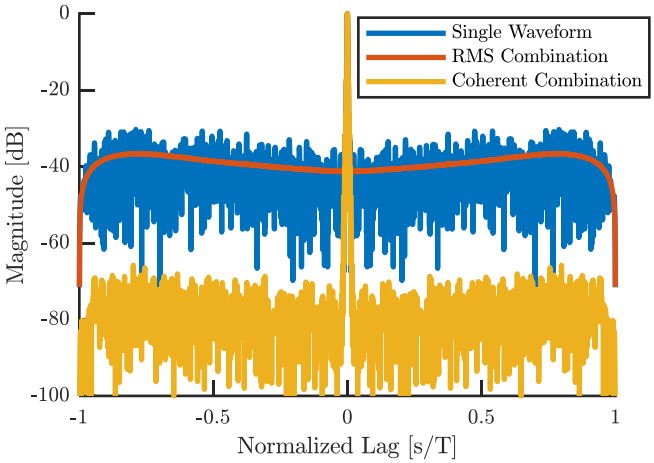

Fig. 5. Loopback autocorrelation results for 5000 unique PRO-FM waveforms generated using $n = 8$

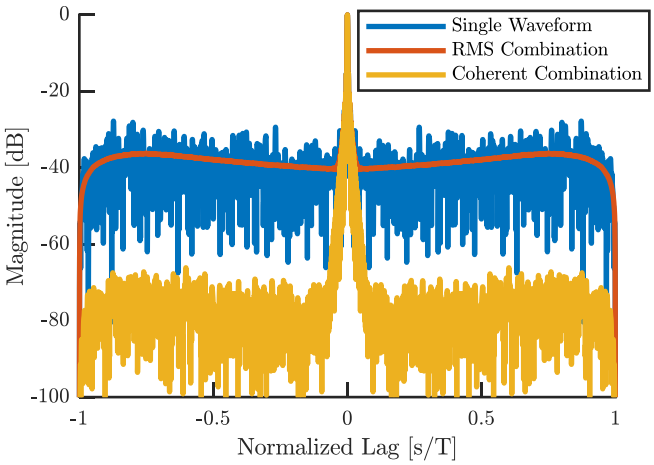

Fig. 6. Loopback autocorrelation results for 5000 unique PRO-FM waveforms generated using $n = 32$

Moreover, as noted in the previous section, additional persistent sidelobes emerge around the mainlobe as the incoherent sidelobe floor is driven down (particularly clear in Fig. 6). Thus, the key take-away is that a sidelobe level proportional to the "aggregate time-bandwidth product" *MTB* is

still achievable when designing for better spectral containment, with the key trade-off being persistent sidelobes, which from a practical perspective can simply be viewed as broadened mainlobe roll-off.

To evaluate cross-correlation performance among each set of RFM waveforms the first waveform in each set was cross-correlated with the other 4999 waveforms, where the "single waveform" (a single result) and the "RMS combination" over the set of 4999 responses are shown in Fig. 7 for the $n = 8$ case. The "coherent combination" (i.e. slow-time combining) over these 4999 cross-correlation responses is likewise depicted, though as we see there is no coherent component since the waveforms are dissimilar. The $n = 2$ and 32 cases realize almost identical responses so are not included. Indeed, peak RMS cross-correlation values obtained are –28.4 dB, –26.6 dB, and –26.1 dB for $n = 2$, 8, and 32, respectively, which have good agreement with previous observations that independent RFM cross-correlation is roughly $-10\log_{10}(TB = 472) = -26.7$ dB.

Like autocorrelation, we see that higher n introduces a modest degradation in cross-correlation, here by 1.8 dB and then another 0.5 dB. However, the benefit of incoherent responses (aside from their autocorrelation mainlobes) again realizes further suppression when slow-time processing is performed, with the coherent combination trace the same $10\log_{10}(5000) = 37$ dB lower than the single waveform result. In other words, there is a small degradation in waveform separability as n increases, but the distinction is essentially negligible for large TB and/or M (e.g. in imaging applications).

It is also important to note that the 60 dB of separability depicted in Fig. 7 does not involve any form of optimization on the basis of cross-correlation. Instead, this result arises solely from the high dimensionality of these unique waveform sets, stemming from the independent random initialization of each waveform and likewise occurring for each RFM method and the broader category of noise radar in general. Indeed, if we compute $10\log_{10}(MTB = 5000\times472) = 63.7$ dB, we again see good agreement on the expected order of separability.

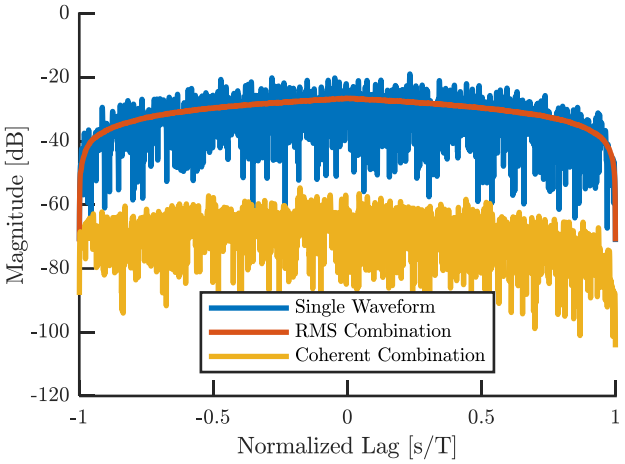

Fig. 7. Loopback cross-correlation results for 5000 unique PRO-FM waveforms generated using $n = 8$

Figs. 8, 9 and 10 subsequently depict the spectral content of each loopback waveform set relative to the particular spectral design template. Because spectral content is predominantly a transmit perspective, a coherent combining trace is not shown, though the single waveform and RMS combinations reveal interesting behavior.

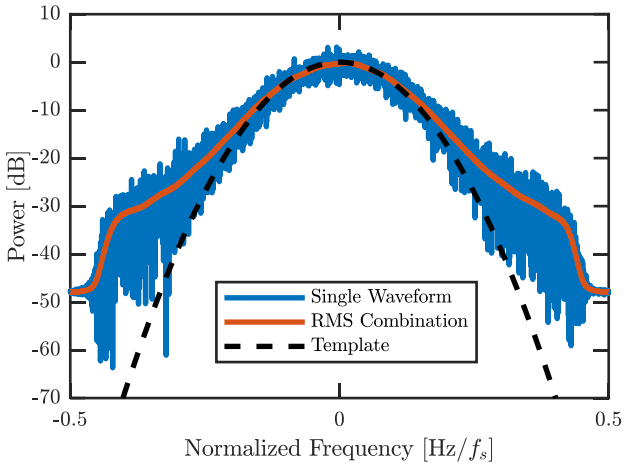

Fig. 8. Loopback spectral content for 5000 unique PRO-FM waveforms generated using $n = 2$

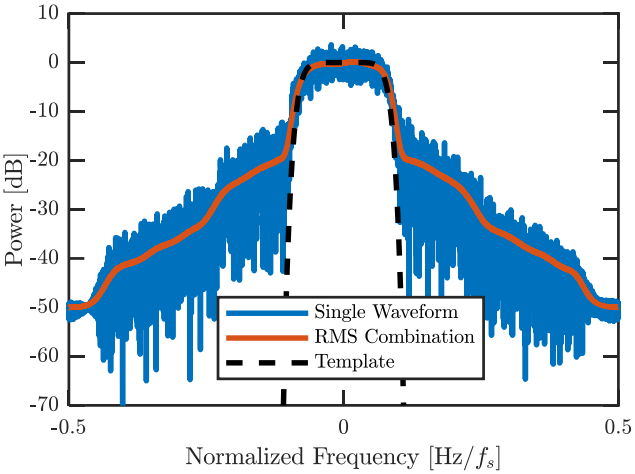

Fig. 9. Loopback spectral content for 5000 unique PRO-FM waveforms generated using $n = 8$

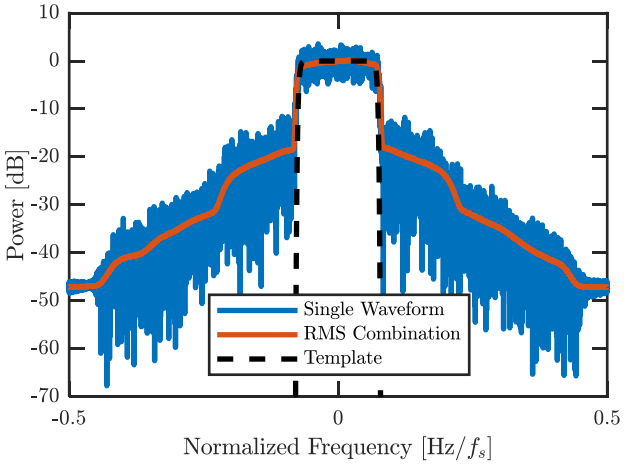

Fig. 10. Loopback spectral content for 5000 unique PRO-FM waveforms generated using $n = 32$

It is first worth noting that both the design templates and RMS results for all three spectra have the same 3-dB bandwidth, even though the n = 2 case in Fig. 8 appears broader, which is due to the more gradual roll-off. If we determine the percentage of power density within this 3-dB bandwidth for the RMS responses, it is found to be 75.1%, 97,5%, and 98.5% for n = 2, 8 and 32, respectively. In other words, higher n provides greater spectral concentration of signal power, not a surprising result given the design templates. In fact, simulation evaluation using RMS responses (again for 5000 unique PRO-FM waveforms in each trial) shows in Fig. 11 that values of n above 12 reach a saturation point of 98.5% in-band power, with the remaining 1.5% likely due to enforcement of a rectangular pulse shape.

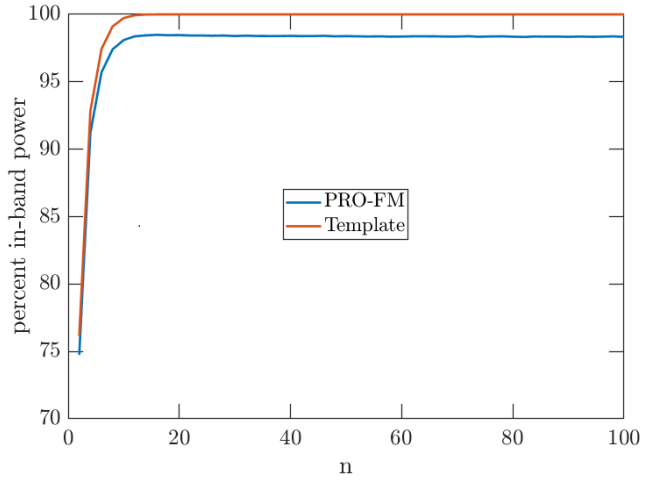

Fig. 11. Simulation of percent power within 3-dB bandwidth versus n for ideal template and RMS response of 5000 PRO-FM waveforms

Where the above percentage is a "vertical" assessment of template error in terms of power deviation, another useful comparison is the point at which the RMS spectrum response in each case deviates from the given template by some nominal amount (i.e. a "horizontal" assessment). Specifically, let 5% of 3-dB bandwidth be the threshold for declaring deviation from the template, which for the n = 2, 8, and 32 spectra respectively translates into −8.3 dB, −14.3 dB, and −18.0 dB relative to the peak. From this perspective, the implication is that higher n not only supports better spectral containment, it also appears to facilitate better template matching.

However, a discrepancy emerges when we alternatively consider the overall percent deviation between each RMS spectrum and its template (another "vertical" assessment), which yields 4.4%, 6.8%, and 7.8% for n = 2, 8, and 32, instead suggesting poorer matching with higher n. These distinctions can be reconciled by variations in the passband for each RMS spectrum, where 4.3%, 6.7%, and 7.7% error is obtained for n = 2, 8 and 32 when only the 3-dB passband is considered. This result indicates that the overwhelming majority of error is contributed by the passband instead of the roll-off region.

It is also worth noting that all three RMS spectra reach a level that is 48-50 dB below the peak at the edges of the displayed normalized frequency interval. However, the n = 8 and 32 cases in Figs. 9 and 10 do so after first providing tighter passband containment, outside of which the roll-off rate appears to reach the limit for RFM waveforms and this hardware configuration. Indeed, the final drop at the outer edge of all three RMS spectra is likely due to the anti-aliasing filter in the real-time spectrum analyzer used here as a receiver, suggesting that the "knee" in each trace is the true transmit spectrum that we are able to capture, with the n = 2 case about 10 dB higher than the other two cases at that point, implying poorer spectral containment as expected for n = 2.

Finally, Fig. 12 shows moving target indication (MTI) results for the n = 8 set of PRO-FM waveforms, which illuminated a traffic intersection in Lawrence, KS from the roof of Nichols Hall on the University of Kansas campus. A -40 dB Taylor window was applied to mitigate Doppler sidelobes and a simple projection at/around zero-Doppler was used for clutter cancellation.

Multiple movers are clearly visible, with this result qualitatively identical to others that have been collected for RFM waveforms (e.g. see [15-17]). While our ultimate goal here is to extend the utility of RFM waveforms for wideband applications, the purpose of this result is simply to show that designing for better spectral containment is likewise useful for MTI and other narrowband applications and does indeed perform as expected for real radar functions.

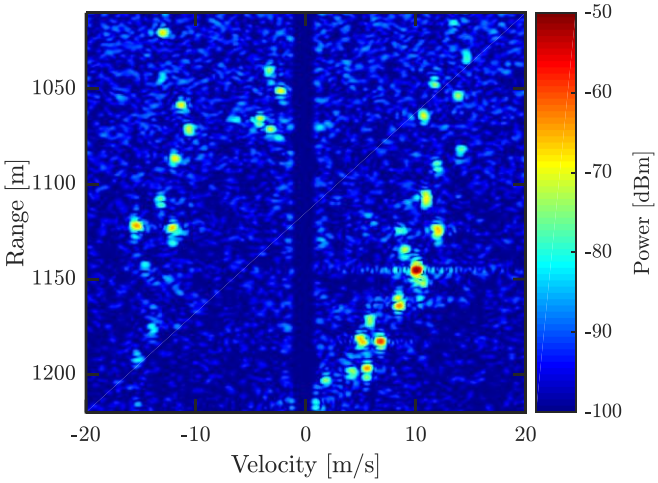

Fig. 12. Open-air range-Doppler response from 5000 unique PRO-FM waveforms generated using n = 8

V. CONCLUSIONS

The super-Gaussian function has been demonstrated experimentally to provide a useful spectral design template for random FM waveforms. Increasing the exponential shape parameter n greater than 2 (Gaussian) yields increasingly tighter spectral containment, which is necessary for extension to wideband operation due to the required inclusion of roll-off to minimize waveform distortion. The trade-offs incurred for better containment include the emergence of persistent range sidelobes close to the mainlobe (though these may be viewed as broadened mainlobe roll-off), a marginal increase in the incoherent sidelobe floor, and a marginal degradation to cross-correlation separability. However, higher n also appears to provide a sharper roll-off outside the design passband spectrum,

thereby suggesting more amenable hardware implementation for wideband operation.

REFERENCES

[1] T.B. Whiteley, D.J. Adrian, “Random FM autocorrelation fuze system,” U.S. Patent #4,220,952, issued 2 Sept. 1980, filed 17 Feb. 1956.

[2] L. Guosui, G. Hong, Z. Xiaohua, S. Weimin, “The present and future of random signal radars,” *IEEE Aerospace & Electronic Systems Mag*., vol. 12, no. 10, pp. 35-40, Oct. 1997.

[3] S.R.J. Axelsson, “Noise radar using random phase and frequency modulation,” *IEEE Trans. Geoscience & Remote Sensing*, vol. 42, no. 11, pp. 2370-2384, Nov. 2004.

[4] L. Pralon, B. Pompeo, J.M. Fortes, “Stochastic analysis of random frequency modulated waveforms for noise radar systems,” *IEEE Trans. Aerospace & Electronic Systems*, vol. 51, no. 2, pp. 1447-1461, Apr. 2015.

[5] G. Beltrao, L. Pralon, A. Barreto, M. Alaee-Kerahroodi, B. Shankar, “Subpulse processing for unambiguous doppler estimation in pulse doppler noise radars,” to appear in *IEEE Trans. Aerospace & Electronic Systems*.

[6] S.D. Blunt, et al., "Principles & applications of random FM radar waveform design," *IEEE Aerospace & Electronic Systems Mag*., vol. 35, no. 10, pp. 20-28, Oct. 2020.

[7] S.D. Blunt, E.L. Mokole, "An overview of radar waveform diversity," *IEEE Aerospace & Electronic Systems Mag*., vol. 31, no. 11, pp. 2-42, Nov. 2016.

[8] S.D. Blunt, M. Cook, J. Jakabosky, J. de Graaf, E. Perrins, "Polyphase-coded FM (PCFM) radar waveforms, part I: implementation," *IEEE Trans. Aerospace & Electronic Systems*, vol. 50, no. 3, pp. 2218-2229, July 2014.

[9] B. Ravenscroft, J.W. Owen, J. Jakabosky, S.D. Blunt, A.F. Martone, K.D. Sherbondy, "Experimental demonstration and analysis of cognitive spectrum sensing & notching," *IET Radar, Sonar & Navigation*, vol. 12, no. 12, pp. 1466-1475, Dec. 2018.

[10] N. Levanon, E. Mozeson, *Radar Signals*, Wiley-IEEE Press, 2004.

[11] X. Xu, R.M. Narayanan, “Range sidelobe suppression technique for coherent ultra wide-band random noise radar imaging,” *IEEE Trans. Antennas & Propagation*, vol. 49, no. 12, pp. 1836-1842, Dec. 2001.

[12] S.R.J. Axelsson, “Random noise radar/sodar with ultrawideband waveforms,” *IEEE Trans. Geoscience & Remote Sensing*, vol. 45, no. 5, pp. 1099-1114, May 2007.

[13] M. Malanowski, K. Kulpa, “Detection of moving targets with continuous-wave noise radar: theory and measurements,” *IEEE Trans. Geoscience & Remote Science*, vol. 50, no. 9, pp. 3502-3509, Sept. 2012.

[14] C.A. Mohr, S.D. Blunt, “Designing random FM radar waveforms with compact spectrum,” *IEEE Intl. Conf. Acoustics, Speech & Signal Processing*, Toronto, Canada, June 2021.

[15] C.A. Mohr, S.D. Blunt, "FM noise waveforms optimized according to a temporal template error (TTE) metric," *IEEE Radar Conf*., Boston, MA, Apr. 2019.

[16] J. Jakabosky, S.D. Blunt, B. Himed, "Spectral-shape optimized FM noise radar for pulse agility," *IEEE Radar Conf*., Philadelphia, PA, May 2016.

[17] C.A. Mohr, P.M. McCormick, S.D. Blunt, C. Mott, "Spectrally-efficient FM noise radar waveforms optimized in the logarithmic domain," *IEEE Radar Conf*., Oklahoma City, OK, Apr. 2018.

[18] A. Parent, M. Morin, P. Lavigne, “Propagation of super-Gaussian field distributions,” *Optical and Quantum Electronics*, vol. 24, no. 9, pp. S1071-S1079, 1992.